Solvent Effects on the S_N2 Reaction: Application of the Density Functional Theory-Based Effective Fragment Potential Method

Ivana Adamovic and Mark S. Gordon*

Department of Chemistry, Iowa State University, Ames, Iowa 50011

Received: October 18, 2004

The performance of the density functional theory (DFT)-based effective fragment potential (EFP) method is assessed using the S_N2 reaction: $Cl^- + nH_2O + CH_3Br = CH_3Cl + Br^- + nH_2O$. The effect of the systematic addition of water molecules on the structures and relative energies of all species involved in the reaction has been studied. The EFP1 method is compared with second-order perturbation theory (MP2) and DFT results for $n = 1$, 2, and 3, and EFP1 results are also presented for four water molecules. The incremental hydration effects on the barrier height are the same for all methods. However, only full MP2 or MP2 with EFP1 solvent molecules are able to provide an accurate treatment of the transition state (TS) and hence the central barriers. Full DFT and DFT with EFP1 solvent molecules both predict central barriers that are too small. The results illustrate that the EFP1-based DFT method gives reliable results when combined with an accurate quantum mechanical (QM) method, so it may be used as an efficient alternative to fully QM methods in the treatment of larger microsolvated systems.

I. Introduction

A. Solvation Methods. An accurate description of solvent effects is very important for understanding many chemical reactions. The two general approaches to solvation, the continuum[1] and discrete[2] methods, are both useful in particular contexts. The continuum methods are fast, and they are mainly designed to represent bulk solvent effects on a solute. Their major disadvantages are that they can be very sensitive to cavity parameters and that they cannot describe the individual interactions between solute and solvent molecules. While discrete methods can treat these interactions accurately, they may have a high intrinsic computational cost and they require extensive configurational sampling for even a modest number of solvent molecules.

For the accurate treatment of individual interactions between solute and solvent molecules, the family of effective fragment potential (EFP1) methods has been developed. In its original formulation, the EFP1[3] method was based on the Hartree−Fock (HF) level of theory. This method (described in detail in ref 4) has been tested extensively in many different applications: treatment of chemical reactions in solution,[5] study of solvent clusters,[6] solvent effects on excited states of biomolecules,[7] neutral−zwitterion equilibrium in amino acids,[8] and treatment of the covalent bond in proteins.[8,9] The EFP1 method has also been interfaced with the polarizable continuum model (PCM)[10] continuum method. All of these applications showed that the HF-based EFP1 method accurately reproduces the corresponding HF results. To include some correlation effects in the EFP1 model, a new DFT-based EFP1[11] implementation was developed. This method is based on density functional theory, using the B3LYP[12,13] functional. A short summary of the DFT-based EFP1 method is given in section II. Since this is a new method, one goal of this study is to demonstrate the accuracy and usefulness of the DFT-based EFP1 method, applying it to the treatment of the solvent effects on a S_N2 chemical reaction.

B. S_N2 Reaction. The S_N2 reaction has been studied extensively both in the gas phase and in solution, because of its great importance in physical organic chemistry and biological systems. It is well-known that the activation barrier for the S_N2 reaction is strongly affected by solvent polarity, and that is the focus of the current work.

Gas-phase S_N2 reactions have been investigated experimentally,[14] by dynamics methods[15] and by ab initio methods.[14a,b,16,17] Many of the gas-phase studies are concerned with determination of the rate constants, secondary α-deuterium kinetic isotope effects (KIEs), and their temperature dependence.[14c,d,15,18] More details on the gas-phase reactions may be found in refs 14−18 and references therein.

While continuum solvent methods[19] provide some general information on the shape of the reaction profile in aqueous solution versus gas-phase systems, the microsolvation approach provides details about the explicit role of specific solvent molecules. Gas-phase experiments[20] on microsolvation processes have provided new insights on many features of S_N2 reactions, for example, rate coefficients, KIEs, and their temperature dependence. Some of the results are in excellent agreement with statistical transition state theory results,[20a] while some[14c] exhibit deviations from transition state theory and represent new theoretical challenges. Since these microsolvated systems bridge the gap between the gas phase and solution, there are a great number of theoretical studies ranging from all ab initio to different types of hybrid quantum mechanics (QM)/molecular mechanics (MM) methods.

Early studies[21] in this field were restricted to $n = 2$ systems, modest basis sets, and levels of theory that do not account for electron correlation, although they provided valuable insights regarding the reaction mechanism. The first QM/MM studies[22] used the TIP4P[23a,b] water potential and Monte Carlo simulations with a large number (∼250) of water molecules. These calculations were followed by Monte Carlo simulations with explicit consideration of $n = 4$ water molecules at the Hartree−Fock level of theory.[24a] The latter study is a very detailed

* Corresponding author.

10.1021/jp040665d CCC: $30.25
Published on Web 02/08/2005

resource of different structures for the $Cl^- + nH_2O + CH_3Cl = CH_3Cl + Cl^- + nH_2O$ reaction. The same system was studied with the B3LYP method with up to four water molecules.[24b] Recent studies on the S_N2 reaction using ab initio molecular dynamics[25] have provided temperature effects, branching ratios, KIEs, and trajectory simulations.

Recently, Re and Morokuma[26] reported a QM/MM study of the reaction $(H_2O)_nCH_3Cl + OH^-(H_2O)_m$ system,[26a] using the ONIOM method.[26b] Their study is similar to the reaction of interest in the present work:

$$Cl^- + nH_2O + CH_3Br = CH_3Cl + Br^- + nH_2O \quad (1)$$

with $n = 1$, 2, 3, and 4.

The primary focus of this work is on the ability of the recently developed DFT-based effective fragment potential (EFP1) method to adequately represent the solvent in an S_N2 reaction. Because the applicability of DFT to S_N2 reactions has been questioned,[16a,25a] the EFP1 solvent calculations have been combined here with both density functional theory and second-order perturbation theory.

II. Theoretical Methods: DFT-Based EFP1 Potential

A detailed description of the DFT-based EFP1 method is given elsewhere;[10] hence, only a brief overview of the method is presented here. In the EFP1 method, one-electron potentials are added to the ab initio electronic Hamiltonian of the solute. These terms represent (a) the electrostatic (Coulombic) interaction between two fragments (EFP−EFP) or between a fragment and a quantum mechanical (e.g. solute) molecule (EFP−QM), screened by a charge penetration function[27] that corrects for overlapping electron densities; (b) the induction (polarization) EFP−EFP or EFP−QM interaction; and (c) a remainder term that contains the exchange repulsion, charge transfer, and higher-order terms that are not contained in the first two terms. The first two terms are determined entirely from QM calculations on the monomer, while the third term is fitted to the QM water dimer potential. The EFP1 formulation may be represented as follows for a solvent molecule μ and a QM coordinate s:

$$V_{el}(\mu, s) = \sum_{k=1}^{K} V_k^{elec}(\mu, s) + \sum_{l=1}^{L} V_l^{pol}(\mu, s) + \sum_{m=1}^{M} V_m^{rep}(\mu, s) \quad (2)$$

The three terms on the right-hand side of eq 2 represent the Coulomb, polarizabilty/induction, and remainder terms, respectively.

The Coulomb interaction is represented by a distributed, multicenter, multipolar expansion[28] (DMA) of the molecular density, using multipoles through octopole moments at $K = 5$ expansion points for the water molecule (nuclear centers and bond midpoints). Since the DMA is a pointwise model, it cannot account for the overlap of the charge densities between two molecules as they approach each other. To correct for this quantum effect, the Coulomb potential is multiplied by a distance dependent cutoff function.

The polarization, or induction, interaction is treated by a self-consistent perturbation model, using localized molecular orbital (LMO) polarizabilities[3]. The molecular polarizability tensor is expressed as a tensor sum of the LMO polarizabilities, centered at the LMO centroids. For water, five such LMOs are used: O inner shell, two O lone pairs, and two O−H bonds. Numerical, finite field calculations, using these LMOs, on an isolated water molecule, provide the total dipole polarizability tensor. The polarization energy is then calculated in a self-consistent manner, by updating the induced dipole as the QM density converges during the self-consistent field (SCF) cycles.

The third term in eq 2 represents the exchange repulsion, charge transfer, and some short-range correlation contributions. This term, for the EFP−QM region is represented as a linear combination of two Gaussian functions expanded at the atom centers. For the EFP−EFP interaction, a single exponential is used and the expansion is done at the atom centers and the center of mass, to better capture the angular dependence of the charge-transfer interaction. The coefficients and exponents of the Gaussian and exponential functions were optimized, by fitting to large numbers of B3LYP water dimer structures, chosen to represent a selection of water−water orientations and O−O distances.[3,10]

The geometry of the fragment water molecule is fixed with bond lengths of 0.9468 Å and a bond angle of 106.70°.[3]

III. Computational Details

All calculations reported in this work were done using the GAMESS[29] electronic structure code. The solute was treated using density functional theory (DFT), employing the B3LYP functional, as well as second-order perturbation theory (MP2).[30] The solvent water molecules were treated with B3LYP, MP2, or the DFT-based EFP1 (from now on called just EFP1) potential. The basis set used in all of these calculations was aug-cc-pVDZ,[31] except for the MP2 gas-phase test calculations that were done with aug-cc-pVTZ,[31] to confirm convergence with respect to the basis set. Most of the geometry optimizations, for up to three water molecules, were done using both B3LYP and MP2 for the entire system, as reference calculations. In addition, several sets of calculations were performed with a QM solute and an EFP solvent: B3LYP solute with EFP1 solvent (DFT-EFP1) and MP2 solute with EFP1 solvent (MP2-EFP1). These calculations provide a test of the reliability of the potential. Relative energies as well as zero point energy (ZPE) corrections are reported for all stationary points. All stationary points along the reaction path were characterized by calculating the force constant (Hessian) matrix. A positive definite Hessian (no negative eigenvalues) corresponds to a local minimum on the potential energy surface (PES). One negative eigenvalue corresponds to a first-order saddle point (transition state). Once the transition states were located, an intrinsic reaction coordinate (IRC)[32] analysis was performed, to ensure that the transition state joins the anticipated two local minima along the PES. As noted in section I, configurational sampling can be important when discrete solvent molecules are used. Location of the global minimum was straightforward for systems with small numbers of water molecules, simply based on chemical intuition. For more than two water molecules, Monte Carlo[33] simulations were employed to help locate global minima. More details about these calculations will be given in section IV.

IV. Results and Discussion

A. Gas-Phase Surface. Gas-phase calculations serve as a benchmark study against which subsequent solvent effects can be assessed. The B3LYP gas-phase results are compared with those based on MP2 in Table 1, and a schematic of the reaction is given in Figure 1. In agreement with previous papers in this general field,[16a,25a] the two methods are in good agreement for relative energies of local minima (reactants, intermediates, and products), but DFT significantly overstabilizes the transition state relative to MP2.

Comparisons of the DFT and MP2 results with previous large basis CCSD(T) calculations[25b] are also given in Table 1. The

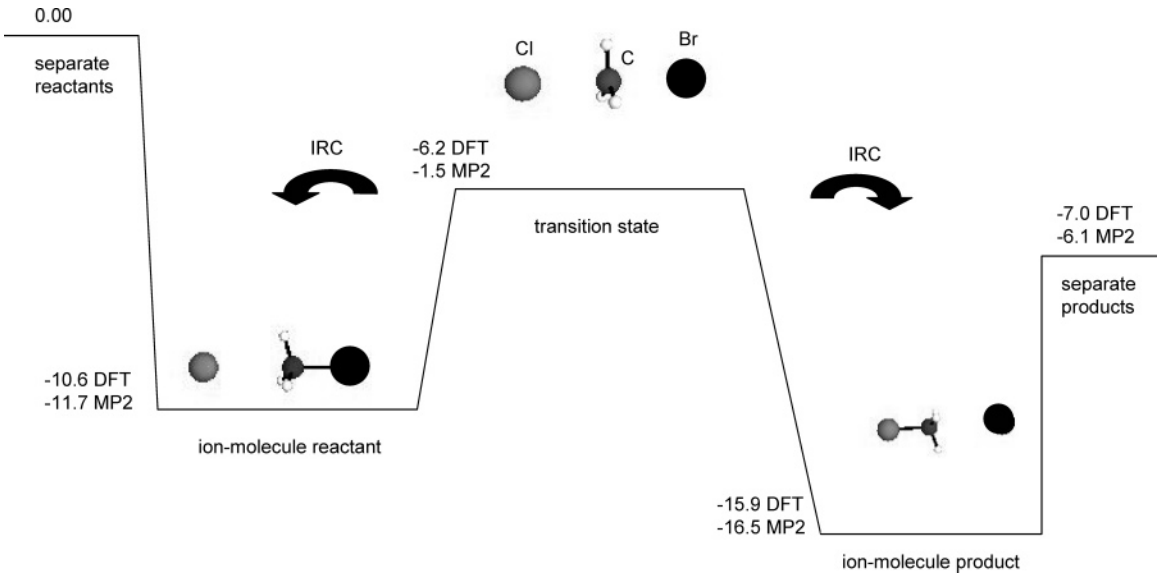

Figure 1. Gas-phase potential energy surface (kcal/mol) for DFT/aug-ccpVDZ and MP2/aug-ccpVDZ.

TABLE 1: Gas-Phase Relative Energies (kcal/mol)

	B3LYP[a]	MP2[a]	CCSD(T)[b]
separate reactants	0.0	0.00	0.00
separate products	−7.0	−6.1 (−6.7)	−8.5
ion pair reactants	−10.6	−11.7 (−11. 4)	−11.3
ion pair products	−15.9	−16.5 (−16. 5)	−18.2
transition state	−6.2	−1.5 (−1.0)	−2.3

[a] aug-cc-pVDZ; aug-cc-pVTZ results are given in parentheses; ZPE included. [b] Reference 22, 257 cGTOs/(s, p, d, f) of the aug-cc-pVQZ for C, Cl and Br/sp (aug-cc-pVTZ) + d (cc-pVTZ) for H.

TABLE 2: Method and Basis Set Convergence with Respect to Imaginary Frequency (cm^{-1})

method/basis set	imaginary frequency
B3LYP/aug-cc-pVDZ	318
MP2/aug-cc-pVDZ	477
MP2/aug-cc-pVTZ	491

MP2 results, including barrier height, agree quite well with the benchmark CCSD(T) studies. The basis set effect on the MP2 energies was investigated by repeating optimizations and Hessian calculations with the aug-cc-pVTZ basis set. The relative MP2 energies for the two basis sets are also given in Table 1, and the imaginary frequencies at the transition state are shown in Table 2. For both energies and frequencies, the influence of the basis set is small. The much smaller B3LYP imaginary frequency reflects the much lower barrier height at this level of theory.

In the following sections, the influence of water molecules on the energy profile shown in Figure 1 is assessed. In view of the small basis set effect in the gas phase, the solvation studies are performed with the smaller aug-cc-pVDZ basis set. In addition to testing the performance of the EFP1 method, it is of interest to determine if the DFT method can capture the influence of the solvent on the barrier heights, despite its flaws in capturing the gas-phase central barrier.

B. One Water Molecule ($n = 1$). The addition of just one water molecule to the system changes the central barrier significantly (Table 3), as shown previously.[22−25] Since water is a very polar solvent, it stabilizes separated small ions and ion−molecule pairs more than the transition state, in which the charge density is more delocalized. Thus, the addition of a water molecule increases the activation barrier. The reacting system including the water molecule was treated with both MP2 and B3LYP. In addition, the water was treated using EFP1, with the rest of the system represented by either MP2 or B3LYP. In each case, once a transition state (TS) was located, IRC runs were performed to connect the TS with reactants and products.

TABLE 3: aug-cc-pVDZ Relative Energies with Respect to Ion−Molecule Reactant for $n = 1$ (kcal/mol, ZPE Corrections Included)

	DFT	DFT-EFP1	MP2	MP2-EFP1
Ion−molecule reactant	0.0	0.0	0.0	0.0
TS	7.8	6.7	14.0	12.6
Ion−molecule product	−3.9	−5.1	−2.5	−4.5

TABLE 4: Imaginary Vibrational Frequencies (cm^{-1})

	DFT	DFT-EFP1	MP2	MP2-EFP1
ν (cm^{-1})	322	324	480	481

Calculated relative energies are summarized in Table 3. The differences for full QM calculations versus QM-EFP1 are small, ranging from 1.1 to 2.0 kcal/mol, for both DFT and MP2 solutes. As expected, the difference between MP2 and DFT is much larger, with the MP2 barriers being ~6.2 kcal/mol higher. Table 4 lists values of the imaginary vibrational frequency using all four of the methods. As for the barrier heights, the QM-EFP1 frequencies are in excellent agreement with the fully quantum values (<2 cm^{-1}), while the significant MP2 versus DFT differences reflect the corresponding differences in E_a.

Figure 2 gives a schematic representation of the reaction path for the $n = 1$ system. As the reaction proceeds from ion−molecule reactants, the $-CH_3$ group translates toward Cl or Br. As the system approaches the ion−molecule product, the water rotates, so that hydrogen bonding is maximized.

C. Two Water Molecules ($n = 2$). The presence of two water molecules in the system can give many different structural arrangements. On the basis of previous studies on the solvation of halogen systems,[34] it is reasonable to expect that the water molecules will tend to cluster and bind first with each other and then with the solute. Indeed the lowest energy transition state (TS) has two water molecules bridging the Cl and Br ends of the TS complex (isomer 1 in Figure 3). Since there are numerous isomers very close in energy, that differ only in their arrangement of the water molecules, additional $n = 2$ isomers are considered in Figure 3. These isomers were chosen using two criteria: (1) low energy structures and (2) to represent different families of isomers in terms of their solvation behavior.

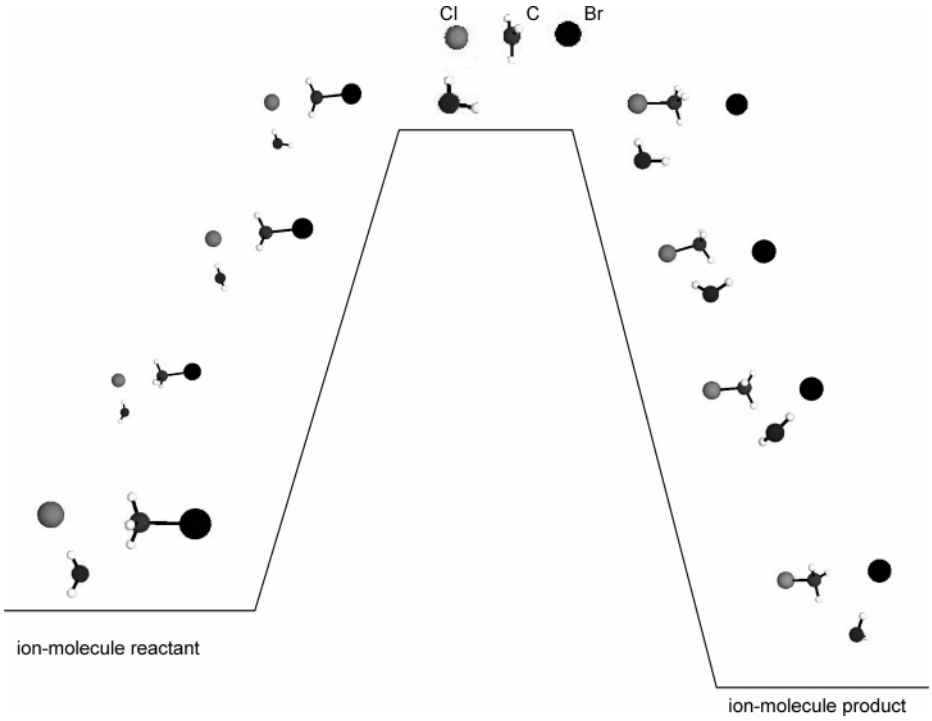

Figure 2. Microsolvated ($n = 1$) potential energy surface: snapshots for the DFT-EFP1 IRC run (picture is similar for MP2-EFP1).

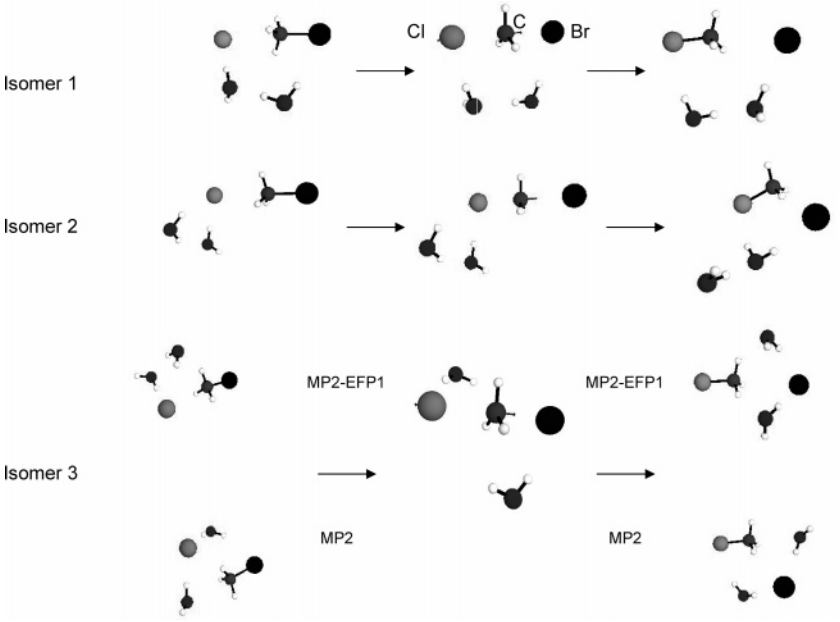

Figure 3. Schematic of the microsolvated ($n = 2$) reaction for isomers 1, 2, and 3.

TABLE 5: Relative Energies (ΔE, kcal/mol) and Imaginary Vibrational Frequencies (ν, cm^{-1}) of the Transition State for $n = 2$ (ZPE Corrections Included)

	DFT	DFT-EFP1	MP2	MP2-EFP1	DFT	DFT-EFP1	MP2	MP2-EFP1	DFT	DFT-EFP1	MP2	MP2-EFP1
ΔE	0.0	0.0	0.0	0.0	0.5	1.5	1.4	1.7	0.6	3.1	2.4	3.2
ν	320	314	474	471	313	325	474	482	318	321	480	482

One of these (isomer 2) has both water molecules located near the Cl region in the TS, forming hydrogen bonds with each other and with Cl. In isomer 3, the water molecules are separated in the TS, with one forming a hydrogen bond with Cl and the other forming a hydrogen bond with Br. For all three TS structures, DFT, MP2, DFT-EFP1, and MP2-EFP1 transition states were optimized, followed by IRC calculations.

The relative energies of these three TS structures together with their imaginary harmonic vibrational frequencies are given in Table 5. All of the methods give the same energy ordering of the isomers, with the lowest energy structure corresponding to the water−water hydrogen-bond bridge from Cl to Br, isomer 1. As for $n = 1$, the mixed QM-EFP1 values track the full QM results for both relative energies and frequencies very well. The biggest discrepancy is 2.5 kcal/mol for isomer 3. In this case, the all MP2 and MP2-EFP1 transition states lead to moderately different reactant and product structures, as may be seen from Figure 3, leading to different relative energies, so a direct

TABLE 6: Relative Energies for $n = 2$ (kcal/mol) (ZPE Included)

		DFT	DFT-EFP1	MP2	MP2-EFP1
isomer 1	ion−molecule reactant	0.0	0.0	0.0	0.0
	TS	9.3	8.4	14. 3	13.1
	ion−molecule product	−3.5	−6.5	−3.1	−5.3
isomer 2	ion−molecule reactant	0.0	0.0	0.0	0.0
	TS	11. 0	10. 9	17. 6	16. 7
	ion−molecule product	−1.3	−2.2	−1.3	−1.5
isomer 3	ion−molecule reactant	0.0	0.0	0.0	0.0
	TS	11. 4	11. 8	17. 3	16. 3
	ion−molecule product	−1.5	−2.8	−2.4	−3.4

comparison is less meaningful. In all cases, the imaginary vibrational frequencies agree to within 3−8 cm^{-1}.

As for one water molecule, as the reaction approaches the ion−molecule complexes, the water molecules orient toward the charged species (Cl or Br), as one would expect (Figure 3).

The central barriers for all three isomers are given in Table 6. The agreement between QM-EFP1 and the corresponding full QM methods is generally very good, with the exception of discrepancies of ∼3 kcal/mol for DFT versus DFT-EFP1 for the products of isomer 1. The addition of two water molecules to the reacting system increases the central barrier, relative to one water (cf. Tables 3 and 6), but the increase is generally smaller than that found for the addition of the first water molecule. The first water molecule increases the barrier by ∼3.4 kcal/mol, while the increase due to the second one is only ∼1.5 kcal/mol. Apparently, the first water molecule stabilizes the ion−molecule pairs sufficiently that the addition of a second water molecule has a similar effect on these local minima and TS. To explore this further, next consider the three-water-molecule case.

D. Three Water Molecules ($n = 3$). Minima and transition state structures for $n = 3$ were determined by starting from structures that have been reported previously[24,35] and then performing Monte Carlo/simulated annealing calculations.[33] These simulations were done using an initial temperature of 500 K, more than enough to overcome the small barriers encountered in these S_N2 reactions. The QM $(Cl - - - CH_3 - - - Br)^-$ part of the system is kept frozen, while the EFP1 water molecules are allowed to move in a box size of 10 × 10 × 10 $Å^3$. The simulations resulted in the TS structures shown in Figure 4, together with the corresponding local minima. While the Monte Carlo searches were extensive, it is, of course, possible that a lower energy TS exists. In the lowest energy TS (isomer 1), the water molecules interconnect through a hydrogen-bonded network, with the hydrogens pointing toward the Cl and Br ends of the complex. The structure is similar to the arrangement of the water trimer,[5a] except that the minimum energy structure in this case has all hydrogens pointing down, to orient toward the negatively charged halogens.

The relative energies and imaginary frequencies for the lowest three TS isomers, that represent different families of isomers, are given in Table 7. All methods give the same ordering of the isomers, with a deviation between QM-EFP1 and the corresponding QM method from 1 to 2.6 kcal/mol. Harmonic imaginary frequencies agree quite well. MP2-EFP1 and MP2 agree to within ∼10 cm^{-1}, while the DFT-EFP1 and DFT agreement is in a range of 20 cm^{-1}.

The central barriers for these three isomers are listed in Table 8. The overall agreement between QM-EFP1 and pure QM results for the central barrier is good. The only exception is the activation energy for isomer 1 with DFT versus DFT-EFP1, for which the deviation is surprisingly ∼5 kcal/mol. The origin of this disagreement is in the different water arrangements in the local minima, at the end of the IRCs, for DFT versus DFT-EFP1. DFT-EFP1 finds a local minimum structure that has strongly connected water molecules (as do the MP2 and MP2-EFP1 methods), while the local minimum structure predicted by DFT has a much weaker binding of water molecules among themselves.

All other systems (including isomer 1 at the MP2 level) show much better agreement for the central barrier. The biggest discrepancy occurs for the ion−molecule product relative energies in isomer 3, ∼6.8 kcal/mol. This disagreement partially comes from a deficiency of the potential itself. In this case, EFP1 predicts water−water binding that is too large and hence overstabilizes the ion−molecule product compared to the ion−molecule reactant. The other source of disagreement arises from differences in ZPE corrections.

It is interesting that, for the lowest energy transition state (isomer 1), the forward barrier is ∼4 kcal/mol *lower* than the lowest energy barrier for $n = 2$ (cf. Table 6), at the same level of theory MP2-EFP1 (MP2, DFT-EFP1). Indeed, this barrier is also lower than that for $n = 1$ and only slightly (∼0.2 kcal/mol) higher than the gas-phase value. In this case, it seems that water molecules are strongly hydrogen bonded to each other, so their cluster configuration does not change from TS to ion−reactant (isomer 1, Figure 4). The interaction energy mostly comes from water−water and not water−solute interactions, so the value of the barrier remains unchanged and is similar to that of the gas-phase reaction. For isomers 2 and 3, the water molecules have a stronger interaction with the Cl and Br ends, so that the forward central barrier behaves as expected for an S_N2 reaction: the central barrier is very similar to the corresponding $n = 2$ isomers. Note that the reverse central barrier

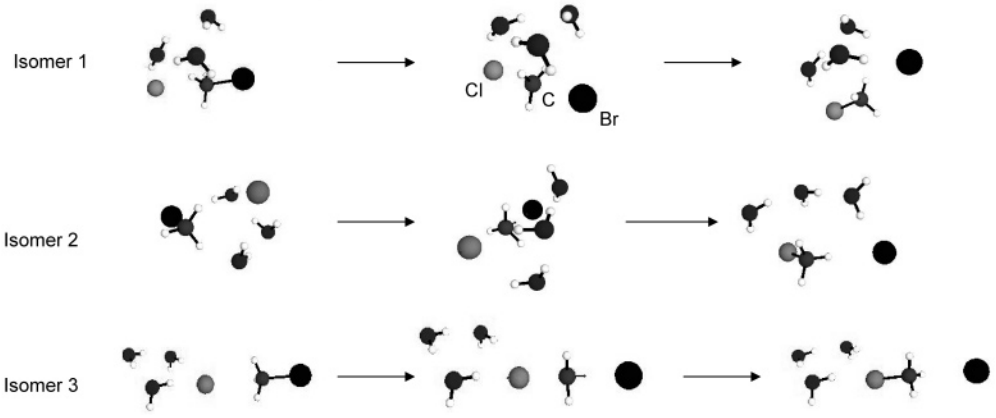

Figure 4. Schematic of the microsolvated ($n = 3$) reaction for isomers 1, 2, and 3.

TABLE 7: Relative Energies (kcal/mol) and Imaginary Vibrational Frequencies (cm^{-1}) of the Transition States for $n = 3$ (ZPE Corrected Values)

	isomer 1				isomer 2				isomer 3			
	DFT	DFT-EFP1	MP2	MP2-EFP1	DFT	DFT-EFP1	MP2	MP2-EFP1	DFT	DFT-EFP1	MP2	MP2-EFP1
ΔE	0.0	0.0	0.0	0.0	0.2	1.5	1.0	1.3	1.2	3.8	4.7	3.7
ν	321	305	467	458	316	297	460	454	277	299	448	461

TABLE 8: Relative Energies for $n = 3$ (kcal/mol; ZPE Included)

		DFT	DFT-EFP1	MP2	MP2-EFP1
isomer 1	ion−molecule reactant	0.0	0.0	0.0	0.0
	TS	9.4	4.5	11.9	10.4
	ion−molecule product	−3.8	−6.0	−5.5	−5.8
isomer 2	ion−molecule reactant	0.0	0.0	0.0	0.0
	TS	11.9	9.8	18.1	16.1
	ion−molecule product	0.0	−0.3	2.4	0.0
isomer 3	ion−molecule reactant	0.0	0.0	0.0	0.0
	TS	14.3	10.4	19.8	16.7
	ion−molecule-product	12.9	7.4	14.0	7.2

for isomer 3 is even smaller than that in the gas phase, because of an unfavorable arrangement of the three water molecules around the Cl (rather than the Br) end of the system.

On the basis of the relative energies for $n = 1$, 2, and 3, it appears that the MP2-EFP1 method is very reliable. It agrees with the full QM results reasonably well, while being much more efficient computationally. Therefore, this QM/MM approach is used in the next section to explore the $n = 4$ system.

E. Four Water Molecules ($n = 4$). For $n = 4$, the search for the global minimum was conducted using Monte Carlo simulations, starting from different initial guesses. The same simulation techniques described above were used. Many TS isomers, which differ in the positions of the four water molecules were located. Snapshots of the Monte Carlo (MC) simulations (lowest energy TS isomers representing different families) are given in Figure 5.

Some of the TS structures found in these MC searches were reported previously either for this S_N2 reaction or for similar systems.[23,24] As for $n = 3$, to the best of our knowledge, the lowest energy TS for the $n = 4$ system has the water molecules in a "cyclic" arrangement (Figure 5, isomer 1). The harmonic imaginary vibrational frequency for this TS is 459.8i cm^{-1}. In the lowest energy TS for $n = 4$, all four hydrogens are pointing down, toward the negatively charged $(Cl \cdots CH_3 \cdots Br)^-$ complex. Figure 6a gives a schematic for the lowest energy TS of the $n = 4$ system. The central barriers in this case are 10.4 and 13.9 kcal/mol for the forward and reverse reaction, respectively. The central barriers are very similar to those for $n = 3$. As in the $n = 3$ system, the water molecules tend to cluster and interact with each other, in preference to the solute, regardless of how the charge is distributed in the solute, so the relative energies of the TS and ion−reactant complex are almost the same as those in the gas phase. It is unlikely that this type of behavior predominates in solution. For example, water molecules exhibit similar behavior in the presence of simple ions[36] until n reaches 12−20.

As in the $n = 3$ system, TS isomers do exist that exhibit the expected increase in the central barrier. A good example of such behavior is TS isomer 5 (Figure 5). At the MP2-EFP1 level of theory, this TS has forward and reverse barriers of 18.0 and 17.4 kcal/mol, respectively, and its harmonic imaginary frequency is 454i cm^{-1}. A schematic of the S_N2 reaction for isomer 5 is given in Figure 6b. Here, the water molecules change their "interaction sphere" as the reaction proceeds. For example, the water labeled X in Figure 6b interacts with the Cl^- in the ion−reactant complex, with both Cl^- and Br^- in the TS complex, and just with the Br^- in the ion−product complex. In contrast, in TS isomer 1, solvent molecules stay tightly connected to each other throughout the entire reaction path. Consequently, reactions such as those typified by isomer 1 have barriers that are very similar to the gas-phase values, and the reaction is almost independent of solvation. Reactions that display the behavior exhibited by isomer 5 have barriers that tend to increase with the number of water molecules. This type of behavior is what has been commonly observed in experimental studies of solvent effects on S_N2 reactions.

F. Comparison of $n = 1$, 2, 3, and 4. Analysis of the successive addition of water molecules to the reaction system

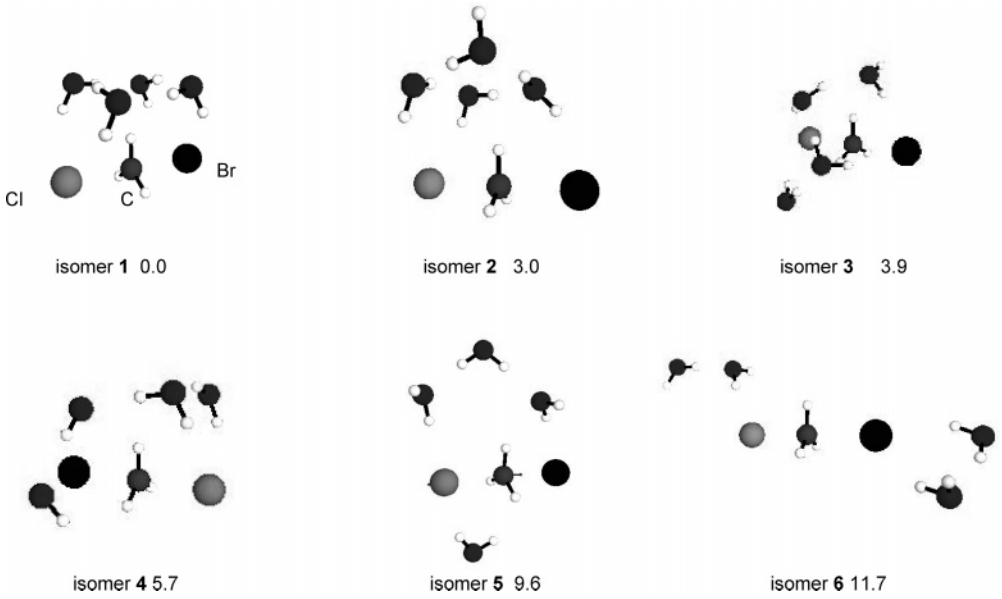

Figure 5. Snapshots of the Monte Carlo simulations: the lowest energy isomers for $n = 4$ (relative energies in kcal/mol, ZPE correction included).

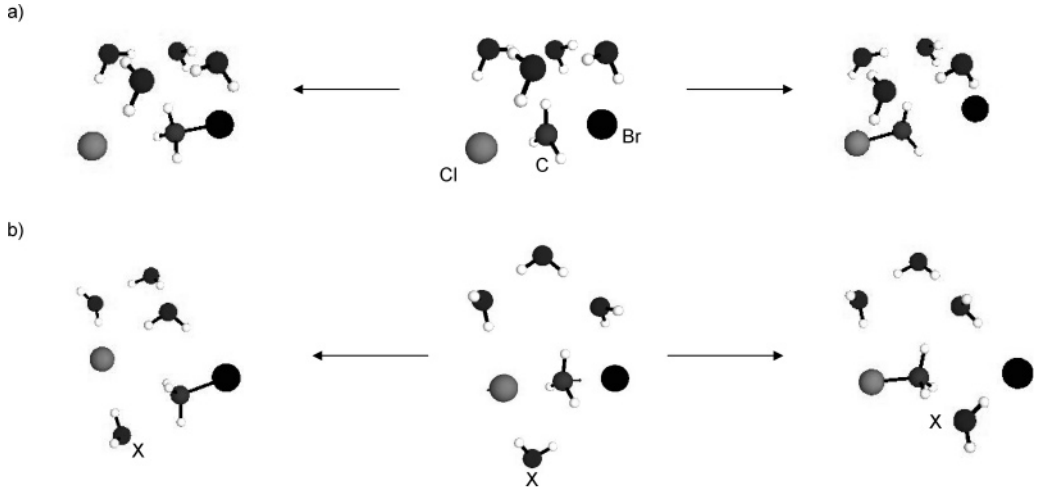

Figure 6. (a) Microsolvated ($n = 4$) potential energy surface for isomer 1 ($n = 4$). (b) Schematic of the potential energy surface for isomer 5 ($n = 4$).

TABLE 9: Forward Central Barrier and Relative Differences as a Function of *n* (kcal/mol) (ZPE Corrected Values)

		forward E_a	ΔE_a
$n = 0$	DFT	4.4	0.0
	DFT-EFP1	6.7	2.3
$n = 1$	DFT	7.8	3.4
	DFT-EFP1	8.4	4.0
$n = 2$	DFT	9.3	4.9
	DFT-EFP1	9.8	5.4
$n = 3$ (isomer 2)	DFT	11.9	7.5
$n = 0$	MP2	10.2	0.0
	MP2-EFP1	12.6	2.4
$n = 1$	MP2	14.0	3.8
	MP2-EFP1	13.1	2.9
$n = 2$	MP2	14.3	4.1
	MP2-EFP1	16.1	5.9
$n = 3$ (isomer 2)	MP2	18.1	7.9
$n = 4$ (isomer 5)	MP2-EFP1	18.0	7.8

leads to some interesting observations. First, in smaller systems, $n = 1$ and 2, the lowest TS isomer exhibits the expected increase of the central barrier compared with the gas-phase value (Tables 3 and 5). Second, in larger systems, $n = 3$ and 4, the lowest energy TS has a central reaction barrier that is similar to that predicted for the gas phase. Depending on the arrangement of the solvent molecules, these larger systems may also exhibit the expected increase in the central barrier height (e.g., isomer 5 for $n = 4$ or isomers 2 and 3 for $n = 3$), with the number of solvent molecules.

Table 9 compares the changes in the relative values of the central barrier upon successive addition of water molecules. The results are based on the lowest energy TS structures for $n = 1$ and 2 and isomers 2 and 5 for $n = 3$ and 4, respectively. The second column of Table 9 gives relative barriers (ΔE_a) (gas-phase value subtracted from solvated barrier) as a function of *n*. Although DFT does a poor job of predicting the absolute barriers, the predicted solvent shifts are equally well represented by all methods. The biggest deviation of DFT versus MP2 is ~1.3 kcal/mol, and the average deviation is ~0.6 kcal/mol. Thus, DFT and DFT-EFP1 calculations can be used to study the solvent shifts in S_N2 reactions.

The influence of the addition of solvent molecules on the harmonic imaginary vibrational frequency of the TS is illustrated in Table 10. There is a very small influence of the solvent on the value of the vibrational frequency.

TABLE 10: Vibrational Analysis—Solvent Effect (cm^{-1})

MP2-EFP1	ν (cm^{-1})
$n = 0$	477i
$n = 1$	481i
$n = 2$	471i
$n = 3$	458i
$n = 4$	460i

V. Conclusions

The DFT-based EFP1 method was used to study the $Cl^- + nH_2O + CH_3Br = CH_3Cl + Br^- + nH_2O$ S_N2 reaction. The treatment of water molecules with the EFP1 potential generally preserves the accuracy of a given QM method, while greatly reducing the computational expense. EFP1 gives accurate structures, relative energies, and vibrational frequencies, compared with full QM methods. Large disagreements between QM and the corresponding QM-EFP1 method are rare and can be easily understood when they occur. It is therefore a cost-effective and reliable method for the treatment of chemical reactions with a large ($n > 3$) number of water molecules.

The $n = 1$ and 2 central barriers increase relative to the gas-phase value, while the lowest TSs found for $n = 3$ and 4 have central barriers that are very similar to the gas-phase value. Other transition states have been found for $n = 3$ and 4 that more closely resemble what one would expect in solution; the corresponding barriers follow the expected trend of increasing barrier height with the number of solvent molecules.

B3LYP overbinds the S_N2 TS and as a consequence gives a smaller central barrier, than those predicted by high level ab initio methods (Table 1). However, B3LYP gives reasonable results for the solvent shifts of the central barrier and for the relative energies of the ion−molecule reactant and ion−molecule product complexes. A very effective approach that combines accuracy and efficiency is to treat the solute with MP2/aug-cc-pVDZ, with water molecules represented by EFP1.

Acknowledgment. This work has been supported by a grant from the Air Force Office of Scientific Research. The calculations in this work were performed in part on a IBM workstation cluster made possible by grants from IBM in the form of a Shared University Research grant, the United States Department of Energy, and the United States Air Force Office of Scientific

Research. The authors are grateful to Professor Veronica Bierbaum for suggesting the [Cl^-, Br^-] S_N2 system.

References and Notes

(1) See the following references: (a) Onsager, L. *J. Am. Chem. Soc.* **1936**, *58*, 1486. (b) Cramer, C. J.; Thrular, D. G. In *Reviews in Computational Chemistry*; Boyd, D. B., Lipkowitz, K. B., Eds.; VCH: New York, 1995; Vol. 6. (c) Cramer, C. J.; Thrular, D. G. In *Solvent effects and Chemical reactivity*; Tapia, O., Bertran, J., Eds.; Kluwer Academic Publishers: Dordrecht, The Netherlands, 1996. (d) Tomasi, J.; Perisco, M. *Chem. Rev.* **1994**, *94*, 2027.

(2) See the following references: (a) Warshel, A. *J. Phys. Chem.* **1979**, *83*, 1640. (b) Levy, R. M.; Kitchen, D. B.; Blair, J. T.; Krogh-Jespersen, K. J. *J. Phys. Chem.* **1990**, *94*, 4470. (c) Thole, B. T.; Van Duijnen, P. T. *Theor. Chim. Acta* **1980**, *55*, 307.

(3) Feature Article: Day, P. N.; Jensen, J. H.; Gordon, M. S.; Webb, S. P.; Stevens, W. J.; Krauss, M.; Garmer, D.; Basch H.; Cohen, D. J. *J. Chem. Phys.* **1996**, *105*, 1968.

(4) Gordon, M. S.; Freitag, M. A.; Bandyopadhyay, P.; Jensen, J. H.; Kairys V.; Stevens, W. J. *J. Phys. Chem. A* **2001**, *105*, 293.

(5) (a) Chen, W.; Gordon, M. S. *J. Chem. Phys.* **1996**, *105*, 11081. (b) Webb S. P.; Gordon, M. S. *J. Phys. Chem. A* **1999**, *103*, 1265.

(6) (a) Merrill, G. N.; Gordon, M. S. *J. Phys. Chem. A* **1998**, *102*, 2650. (b) Day, P. N.; Pachter, R.; Gordon M. S.; Merrill, G. N. *J. Chem. Phys.* **2000**, *112*, 2063.

(7) See the following references: (a) Krauss, M. *Comput. Chem.* **1995**, *19*, 199. (b) Krauss, M.; Wladowski, B. D. *Int. J. Quantum Chem.* **1998**, *69*, 11. (c) Krauss, M.; Webb, S. P. *J. Chem. Phys.* **1997**, *107*, 5771.

(8) Li, H.; Hains, W. A.; Everts, J. E.; Robertson, A. D.; Jensen, J. H. *J. Phys. Chem. B* **2002**, *106*, 3486.

(9) (a) Minikis, R. M.; Kairys V.; Jensen, J. H. *J. Phys. Chem. A* **2001**, *105*, 3829. (b) Molina, P. A.; Sikorski, S. R.; Jensen, J. H. *Theor. Chem. Acc.* **2003**, *109*, 100.

(10) (a) Bandyopadhyay P.; Gordon, M. S. *J. Chem. Phys.* **2000**, *113*, 1104. (b) Bandyopadhyay, P.; Gordon, M. S.; Mennucci, B.; Tomasi, J. *J. Chem. Phys.* **2002**, *116*, 12.

(11) Adamovic, I.; Freitag M. A.; Gordon, M. S. *J. Chem. Phys.* **2003**, *118*, 6725.

(12) (a) Becke, A. D. *Phys. Rev. A* **1988**, *38*, 3098. (b) Lee, C.; Yang W.; Parr, R. G. *Phys. Rev. B* **1988**, *37*, 785.

(13) B3LYP in GAMESS is hybridized HF/Becke/LYP with VWN5. For more details and references, consult the GAMESS manual: http://www.msg.ameslab.gov/GAMESS/doc.menu.html.

(14) (a) Hase, W. H. *Science* **1994**, *266*, 998 and references therein. (b) Chabinyc, M. L.; Craig, S. L.; Regan C. K.; Brauman J. I. *Science* **1998**, *279*, 1882 and references therein. (c) Barlow, S. E.; Van Doren J. M.; Bierbaum, V. M. *J. Am. Chem. Soc.* **1988**, *110*, 7240. (d) Gronert, S.; DePuy, C. H.; Bierboum, V. M. *J. Am. Chem. Soc.* **1991**, *113*, 4009. (e) Kato, S.; Davico, G. E.; Lee, H. S.; DePuy, C. H.; Bierbaum, V. M. *Int. J. Mass. Spectrom.* **2001**, *210*/*211*, 223.

(15) (a) Gonzales-Lafont, A.; Truong T. N.; Truhlar, D. G. *J. Phys. Chem.* **1991**, *95*, 4618. (b) Zhao, X. G.; Tucker S.; Truhlar, D. G. *J. Am. Chem. Soc.* **1991**, *113*, 826. (c) Viggiano, A. A.; Paschkewitz, J. S.; Morris, R. A.; Paulson, J. F.; Gonzales-Lafont A.; Truhlar, D. G. *J. Am. Chem. Soc.* **1991**, *113*, 9404. (d) Ho W.-P.; Truhlar, D. G. *J. Am. Chem. Soc.* **1995**, *117*, 10726. (e) Haobin, W.; Goldfield E. M.; Hase, W. L. *J. Chem. Soc., Faraday Trans.* **1997**, *93*, 737.

(16) (a) Glukhovtsev, M. N.; Pross, A.; Radom, L. *J. Am. Chem. Soc.* **1995**, *117*, 2024. (b) Glukhovtsev, M. N.; Pross, A.; Schlegel, H. B.; Bach R. D.; Radom, L. *J. Am. Chem. Soc.* **1996**, *118*, 11258. (c) Hu W.-P.; Truhlar, D. G. *J. Am. Chem. Soc.* **1994**, *116*, 7797. (d) Deng, L.; Branchadell V.; Ziegler, T. *J. Am. Chem. Soc.* **1994**, *116*, 10645.

(17) Schmatz, S.; Botschwina, P.; Stoll, H. *Int. J. Mass. Spectrom.* **2000**, *201*, 277.

(18) (a) Wang, H.; Hase, W. *J. Am. Chem. Soc.* **1995**, *117*, 9347. (b) Wang, Y.; Hase, W. L.; Wang, H. *J. Chem. Phys.* **2003**, *118*, 2688.

(19) (a) Kozaki, T.; Morihashi, K.; Kikuchi, O. *J. Am. Chem. Soc.* **1989**, *111*, 1547. (b) Cossi, M.; Adamo, C.; Barone, V. *Chem. Phys. Lett.* **1998**, *297*, 1.

(20) (a) O'Hair, R. A. J.; Davico, G. E.; Hacaloglu, J.; Dang, T. T.; DePuy, C. H.; Bierbaum, V. M. *J. Am. Chem. Soc.* **1994**, *116*, 5609. (b) Seeley, J. V.; Morris, R. A.; Viggiano, A. A.; Wang, H.; Hase, W. L. *J. Am. Chem. Soc.* **1997**, *119*, 577.

(21) (a) Morokuma, K. *J. Am. Chem. Soc.* **1982**, *104*, 3732. (b) Ohta, K.; Morokuma, K. *J. Phys. Chem.* **1985**, *89*, 5845. (c) Hirao, K.; Kebarle, P. *Can. J. Chem.* **1989**, *67*, 1261.

(22) (a) Chandrasekhar, J.; S. F. Smith, S. F.; Jorgensen, W. L. *J. Am. Chem. Soc.* **1984**, *106*, 3050. (b) Chandrasekhar, J.; Smith, S. F.; Jorgensen, W. L. *J. Am. Chem. Soc.* **1985**, *107*, 154.

(23) (a) Jorgensen, W. L.; Chandrasekhar, J.; Madura, J. D.; Impey, R. W.; Klein, M. L. *J. Chem. Phys.* **1983**, *79*, 926. (b) Jorgensen, W. L.; Madura, J. D. *Mol. Phys.* **1985**, *56*, 1381.

(24) (a) Okuno, Y. *J. Chem. Phys.* **1996**, *105* (14), 5817. (b) Mohamed, A. A.; Jensen, F. *J. Phys. Chem. A* **2001**, *105*, 3259.

(25) (a) Raugei, S.; Cardini, G.; Schettino, V. *J. Chem. Phys.* **2001**, *114* (9), 4089. (b) Schmatz, S.; Botschwina, P.; Stoll, H. *Int. J. Mass. Spectrom.* **2000**, *201*, 277. (c) Schmatz, S. *Chem. Phys. Lett.* **2000**, *330*, 188.

(26) (a) Re, S.; Morokuma, K. *J. Phys. Chem. A* **2001**, *105*, 7185. (b) Morokuma, K. *Bull. Korean Chem. Soc.* **2003**, *24*, 797 and references therein.

(27) (a) Freitag, M. A.; Gordon, M. S.; Jensen, J. H.; Stevens, W. J. *J. Chem. Phys.* **2000**, *112* (17), 7300.

(28) Stone, A. J. *Chem. Phys. Lett.* **1981**, *83*, 233. (b) Stone, A. J. *The Theory of Intermolecular Forces*; Oxford University Press: Oxford, U.K., 1996.

(29) Schmidt, M. W.; Baldridge, K. K.; Boatz, J. A.; Elbert, S. T.; Gordon, M. S.; Jensen, J. H.; Koseki, S.; Matsunaga, N.; Nguyen, K. A.; Su, S.; Windus, T. L.; Dupuis, M.; Montgomery, J. A., Jr. *J. Comput. Chem.* **1993**, *14*, 1347.

(30) Moller, C.; Plesset, M. S. *Phys. Rev.* **1934**, *46*, 618.

(31) (a) Dunning, T. H., Jr. *J. Chem. Phys.* **1989**, *90*, 1007. (b) Woon D. E.; Dunning, T. H., Jr. *J. Chem. Phys.* **1993**, *98*, 1358. (c) Kendall, R. A., Dunning, T. H., Jr.; Harrison, R. J. *J. Chem. Phys.* **1992**, *96*, 6769. (d) Woon, D. E.; Dunning, T. H., Jr. *J. Chem. Phys.* **1993**, *98*, 1358.

(32) Gonzalez, C.; Schlegel, B. H. *J. Phys. Chem.* **1990**, *94*, 5523.

(33) (a) Parks, G. T. *Nucl. Technol.* **1990**, *89*, 233. (b) Metropolis, N.; Rosenbluth A.; Teller, A. *J. Chem. Phys.* **1953**, *21*, 1087. (c) Li, Z.; Scheraga, H. A. *Proc. Natl. Acad. Sci. U.S.A.* **1987**, *84*, 6611.

(34) Xantheas, S. S.; Dunning, T. H., Jr. *J. Chem. Phys.* **1994**, *98*, 13489.

(35) Xantheas, S. S. *J. Am. Chem. Soc.* **1995**, *117*, 10373.

(36) Kemp, D.; Gordon, M. S. Manuscript in preparation.